Bispherical Force Computation.

An exact solution for the image force can be derived analytically in the bispherical coordinate system due to the isosurfaces that naturally correspond to the sphere/plane geometry. The bispherical coordinate system is described by three orthogonal coordinates, η, θ, and φ. A 2-D projection of the coordinate isosurfaces is depicted in Figure 1 for which φ=0.

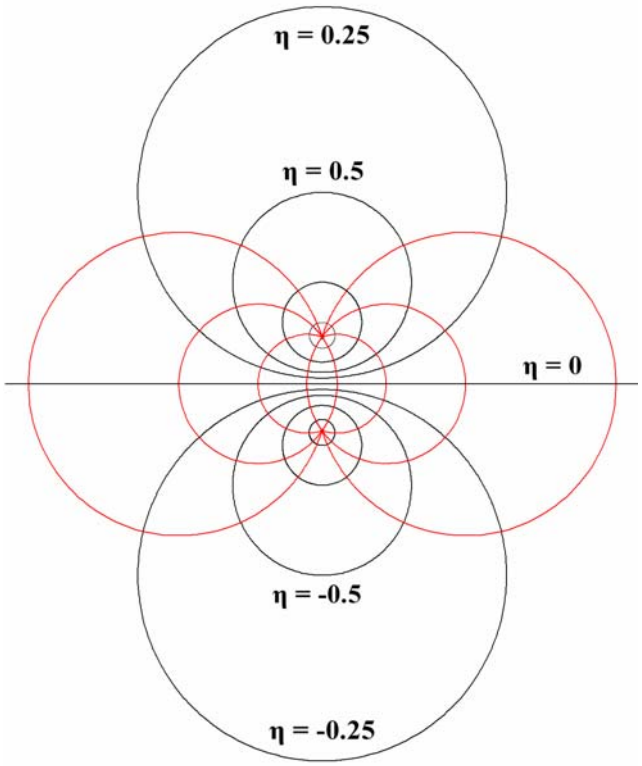

Supplementary Figure 1. *Isosurfaces of constant η (black) and constant θ (red) are presented for φ=0. The constant η isosurfaces represent circles with different radii of curvature. The η=0 isosurface is a circle of infinite radius, whereas η=±∞ are circles of zero radius and located at the two poles. The sphere/plane interaction can be represented by choosing η to scale with the relative sphere/plane separation distance.*

Unlike the most common 11 separable coordinate systems, the bispherical coordinate system is only *R* separable with a general solution for the potential, given by:

$$\varphi(\eta,\theta,\phi) = R(\eta,\theta)H(\eta)\Theta(\theta)\Phi(\phi)$$

where $R(\eta,\theta)=\sqrt{\cosh(\eta)-\cos(\theta)}$. The independent coordinate functions are determined through separation of variables:

$$H(\eta)=E_n e^{-\eta(n+1/2)}+F_n e^{\eta(n+1/2)}$$
$$\Theta(\theta)=K_n^m P_n^m\cos(\theta)+L_n^m Q_n^m\cos(\theta)$$
$$\Phi(\phi)=S_m\sin(m\varphi)+T_m\cos(m\varphi)$$

where P_n^m and Q_n^m are associated Legendre Polynomials of the first and second kinds. Due to the presence of logarithmic singularities in Q_n^m, the L_n^m terms are set to zero. In axially symmetric problems such as this one, we can also set $m=0$, in which case the S_m terms are discarded. For two particles of arbitrary radii, which are defined by surfaces η_1 and η_2, the potential inside particles 1 and 2 and the fluid medium, respectively, are given by:

$$\varphi_1(\eta\geq\eta_1)=H_{ext}z+H_{ext}aR(\eta,\theta)\sum_{n=0}^{\infty}\left(A_n+B_n e^{(2n+1)\eta_1}\right)e^{-(n+1/2)\eta}P_n(\cos\theta)$$

$$\varphi_f(-\eta_2\leq\eta\leq\eta_1)=H_{ext}z+H_{ext}aR(\eta,\theta)\sum_{n=0}^{\infty}\left(A_n e^{-(n+1/2)\eta}+B_n e^{(n+1/2)\eta}\right)P_n(\cos\theta)$$

$$\varphi_2(\eta\leq-\eta_2)=H_{ext}z+H_{ext}aR(\eta,\theta)\sum_{n=0}^{\infty}\left(A_n e^{(2n+1)\eta_2}+B_n\right)e^{(n+1/2)\eta}P_n(\cos\theta)$$

where $a=\sqrt{(1/4)\left(D^2-R_1^2-R_2^2\right)^2-R_1^2R_2^2}\,/D$, R_1 and R_2 are the radii of the first and second spheres, and D is the center-to-center separation distance. The unknowns A_n and B_n are determined by matching with the boundary conditions (e.g., the potential is single-valued everywhere, and the normal component of the flux density, $\vec{B}\cdot\hat{n}$, is continuous across all interfaces). It is possible to solve the image force problem by representing particle 2 as a half-plane with $\eta_2=0$; however due to convergence issues we have chosen a different approach based on the work of Love[1], who showed that the half-plane can be treated as a fictitious sphere[2]

of identical size ($\eta_1 = -\eta_2$) and with coefficients A_n and B_n linked together through the relationship:

$$A_n = -\frac{\mu_f - \mu_s}{\mu_f + \mu_s} B_n$$

Due to the *R*-separable nature of the solution, the orthogonality condition is not satisfied and we must employ Legendre polynomial identities in order to remove the angular dependence from the problem. The following identities are used:

$$\int_{-1}^{1} \left(P_n(x)\right)^2 dx = \frac{2}{2n+1}\delta_{n,n}$$

$$\int_{-1}^{1} xP_n(x)P_m(x)dx = \frac{2n}{(2n-1)(2n+1)}\delta_{n-1,m} + \frac{2n+2}{(2n+1)(2n+3)}\delta_{n+1,m}$$

where $\delta_{i,j}$ is the Kronecker delta having the values: $\delta_{i,j} = \begin{Bmatrix} 1 & if & i=j \\ 0 & if & i \neq j \end{Bmatrix}$

The resulting expressions lead to a series of three term recursion relationships between coefficients A_{n+1}, A_n, A_{n-1}. Many past works have described different numerical approaches for solving these recursion relationships[1, 3, 4]. For convenience, we follow the approach developed by Stoy[3]. Once the coefficients A_n are computed, the potential, fields, and field gradients can be determined. The force on the sphere in the z-direction (away from the surface) is computed from the Maxwell Stress Tensor using the expanded form:

$$F_z = \int_0^{\pi} \frac{2\pi\mu_0 a^2 \sin(\theta)}{(\cosh(\eta)-\cos(\theta))^2}\left[\left(\frac{H_\eta^2 - H_\theta^2}{2}\right)\left(\frac{\cosh(\eta)\cos(\theta)-1}{\cosh(\eta)-\cos(\theta)}\right) + \left(H_\eta H_\theta\right)\left(\frac{\sinh(\eta)\sin(\theta)}{\cosh(\eta)-\cos(\theta)}\right)\right]d\theta$$

where the magnetic fields are determined from the negative gradient of the potential:

$$\vec{H} = \begin{bmatrix} H_\eta \hat{\eta} \\ H_\theta \hat{\theta} \end{bmatrix} = -\left(\frac{\cosh(\eta)-\cos(\theta)}{a}\right)\begin{bmatrix} \frac{d\varphi}{d\eta}\hat{\eta} \\ \frac{d\varphi}{d\theta}\hat{\theta} \end{bmatrix}$$

In Supplementary Figure 2, we plot the ratio of the computed bispherical force with the approximate image dipole force as a function of the sphere/plane separation distance. These simulations assumed that μ_f = 1.66 based on fitting parameters obtained through confocal microscopy. The two forces differ by less than 1% when the sphere/plane separation distance is greater than the sphere radius. At very small separations (down to 1/100th of a sphere diameter), the bispherical force converges to a fixed value that is ~10% greater than the image dipole force calculation. Calculations by others have also shown that the sphere/plane force approaches a limiting value as the separation distance approaches zero[5, 6]. We thus conclude that the image dipole force approximation will lead to a slight underestimation (<10% for μ_f=1.66) of the exact magnetic force on a colloid in contact with a surface.

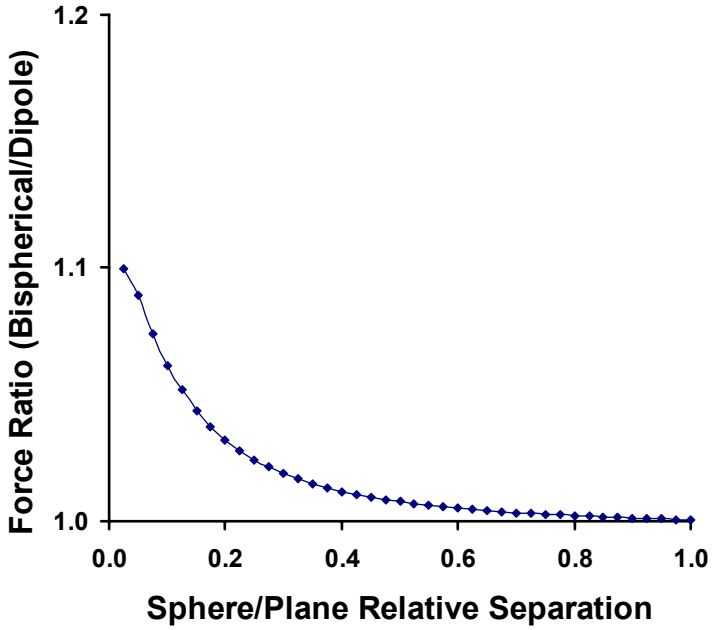

Supplementary Figure 2. *The ratio of force calculated from bispherical coordinates and image dipole force is plotted as a function of the relative sphere/plane separation.*

Sedimentation Analysis

First, the density of the ferrofluid was determined by measuring the mass of a 500μL aliquot of ferrofluid taken directly from the stock volume. The mass density of the ferrofluid was found to be 1.19gm/cc which is in agreement with manufacturer specifications. The mean density of the colloidal beads was subsequently determined through a sink/float analysis. In this technique, the beads were mixed with different concentrations of ferrofluid diluted in water, and microscopy images were taken to determine the ferrofluid concentrations at which the beads sunk to the bottom surface or floated to the top surface. Images were taken in both upright and inverted microscopy, and the results are presented in Supplementary Figure 3 along with the estimated volume fraction of ferrofluid. According to the vendor specifications, the bulk volume fraction of ferrofluid was 3.9%. Our analysis indicated that the mean density of the beads was 1.047g/cc, which agrees well with the actual density of polystyrene beads (1.05g/cc). These mass density values were used in the force balance to estimate the ferrofluid permeability.

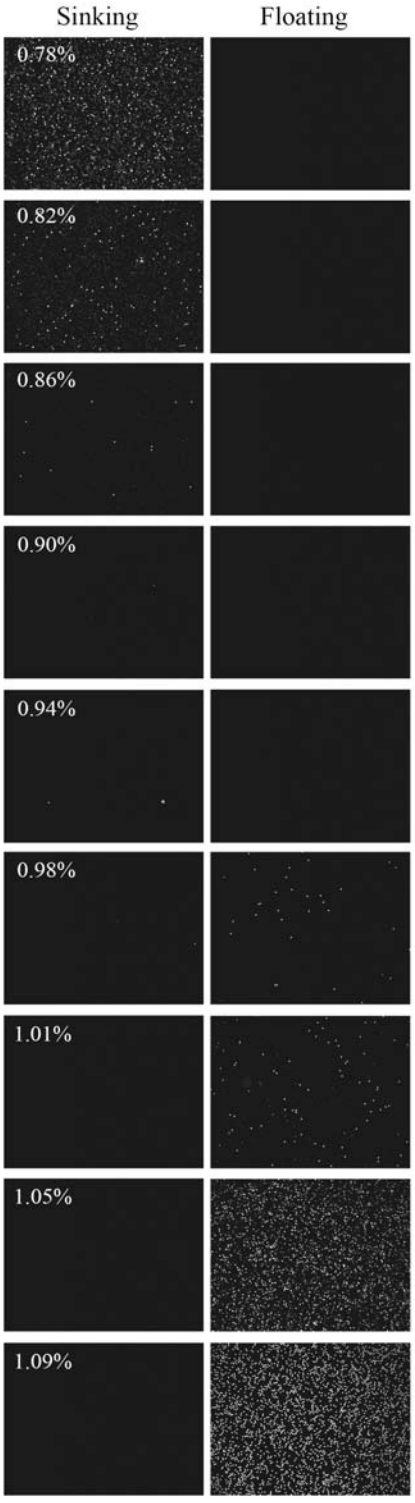

Supplementary Figure 3. *Microscopy images of beads in upright and inverted microscope as a function of the ferrofluid/water mixing ratio.*

Surface Roughness Measurements

Since the surface force measurements were much smaller than expected by theoretical predictions of the sphere/plane Van der Waals interaction, we speculated that an adsorbed ferrofluid layer was coating the bead, causing it to be placed further from the surface. In order to ascertain the validity of this assumption, we performed atomic force microscopy on the surface of a bead that was previously immersed in ferrofluid. Our past experiments have shown that ferrofluid can adsorb onto colloidal beads. See for example the SEM image, provided in Supplementary Figure 4a, which can be found in one of our previous papers[7]. The fit between theory and experiment indicated that the sphere/plane separation distance was on the order of 50nm. This is consistent with AFM height image (Supplementary Figure 4b) which shows a 1-μm area section of the top surface of the bead with the adsorbed ferrofluid layer.

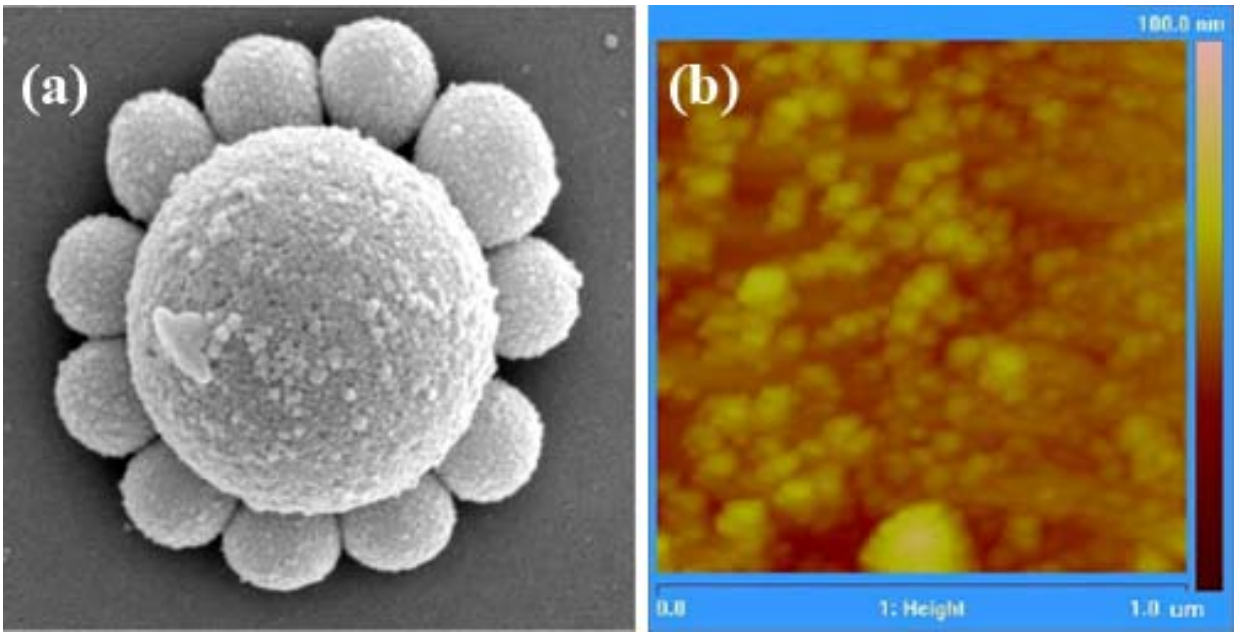

Supplementary Figure 4. *(a) SEM image of a colloidal bead arrangement that was assembled inside ferrofluid. The rough surface demonstrates the adsorption of ferrofluid onto the colloidal beads. (b) A high resolution AFM height image shows the surface roughness of the bead is quite large due to ferrofluid adsorption.*

Estimation of Unbinding Force

Fluorescent intensity measurements and image analysis techniques were used in conjunction to determine the frame at which each bead popped off the surface. All beads within a field of view of a 5X objective were measured, except for beads that were within 4-5 bead diameters of another bead, for which bead-bead magnetic interactions are non-negligible. The experimental results for the 0.0074 pN/s loading rate data are provided in Supplementary Figure 5a along with the fluorescent time signature for a single bead provided in Supplementary Figure 5b. The frame where the bead's fluorescent intensity suddenly decreased was identified as the unbinding frame. The unbinding force for each bead was determined from Equation (1) in the main text and the frame rate.

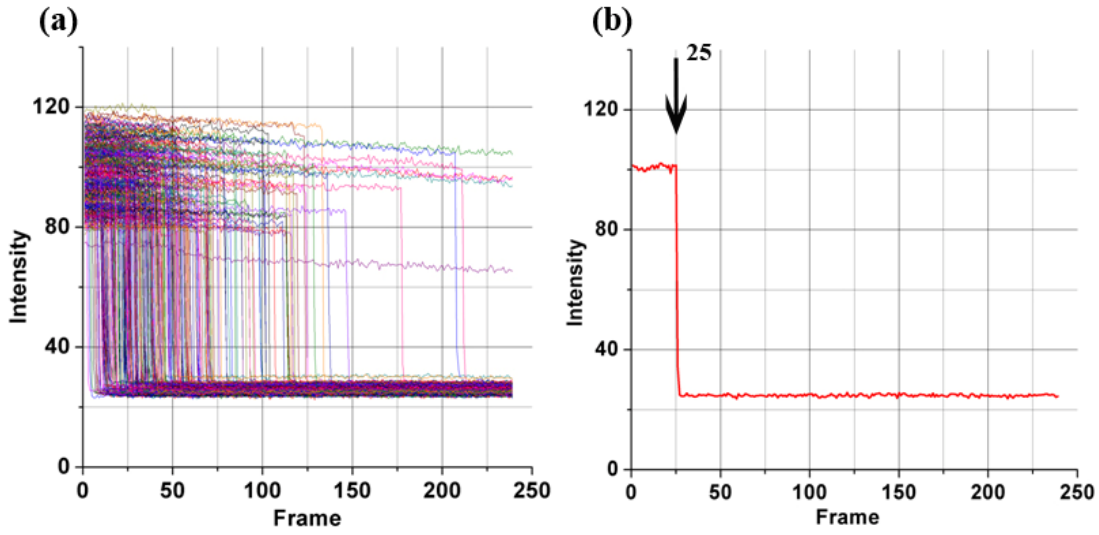

Supplementary Figure 5. *(a) Fluorescent intensity measurements of an ensemble of beads are shown for 0.0074 pn/s loading rate. (b) The fluorescent intensity of a single bead is provided as a function of the frame number and the arrow denotes the unbinding frame.*

Surface Contact Angle Measurements

PEG surfaces before and after irradiation with 254nm UV light (Migge, Heidelberg, Germany) were analyzed through surface contact angle measurements using a contact angle goniometer (Ramé-Hart, Mountain Lakes, NJ). A drop of water was placed onto the surface and was allowed to rest for 1 minute. The contact angle between the drop surface and the substrate was measured four times, and the mean contact angle between water and PEG coated surface was determined to be $7.88°$, with a standard deviation of $1.38°$, whereas the same measurement for the irradiated sample was $7.75°$, with a standard deviation of $0.64°$. Since an inaccuracy of $1° - 2°$ is always present in these measurements, the contact angle of these two different surfaces are indistinguishable, which indicates little difference in the surface energy. With our surface force measurement technique, on the other hand, a very small change could be observed.

References

1. Love, J.D. Dielectric sphere-sphere and sphere-plane problems in electrostatics. *Quart. J. Mech. Appl. Math.* **28**, 448-471 (1975).
2. Erb, R.M. & Yellen, B.B. Model of Detecting Nonmagnetic Cavities in Ferrofluid for Biological Sensing Applications. *IEEE Transactions on Magnetics* **42**, 3554-3556 (2006).
3. Stoy, R.D. Solution procedure for the Laplace equation in bispherical coordinates for two spheres in a uniform external field: Parallel orientation. *Journal of Applied Physics* **65**, 2611-2615 (1989).
4. Chaumet, P.C. & Dufour, J.P. Electric potential and field between two different spheres. *Journal of Electrostatics* **43**, 145-159 (1998).
5. Liu, H. & Bau, H.H. *Phys. Fluids* **16**, 1217 (2004).
6. Young, E.W.K. & Li, D. Dielectrophoretic Force on a Sphere near a Planar Boundary. *Langmuir* **21**, 12037-12046 (2005).
7. Erb, R.M., Son, H.S., Samanta, B., Rotello, V.M. & Yellen, B.B. Magnetic assembly of colloidal superstructures with multipolar symmetry *Nature* **457**, 999-1002 (2009).